FEBS Letters

FEBS PRESS science publishing by scientists

RESEARCH ARTICLE

Polyoxovanadates as new P-glycoprotein inhibitors: insights into the mechanism of inhibition

Diogo Henrique Kita[1,2], Gisele Alves de Andrade[1], Juliana Morais Missina[3], Kahoana Postal[3], Viktor Kalbermatter Boell[3], Francielli Sousa Santana[3], Ingrid Fatima Zattoni[1], Isadora da Silva Zanzarini[1], Vivian Rotuno Moure[1,4], Fabiane Gomes de Moraes Rego[4], Geraldo Picheth[4], Emanuel Maltempi de Souza[5], David A. Mitchell[5], Suresh V. Ambudkar[2], Giovana Gioppo Nunes[3] and Glaucio Valdameri[1,4]

1 Pharmaceutical Sciences Graduate Program, Laboratory of Cancer Drug Resistance, Federal University of Paraná, Curitiba, Brazil
2 Laboratory of Cell Biology, Center for Cancer Research, National Cancer Institute, National Institutes of Health, Bethesda, MD, USA
3 Department of Chemistry, Federal University of Paraná, Curitiba, Brazil
4 Department of Clinical Analysis, Federal University of Paraná, Curitiba, Brazil
5 Department of Biochemistry and Molecular Biology, Federal University of Paraná, Curitiba, Brazil

Correspondence
G. G. Nunes, Department of Chemistry, Federal University of Paraná, Rua Prefeito Lothário Meissner, 632, Jardim Botânico, Curitiba, PR 80210-170, Brazil
E-mail: nunesgg@ufpr.br
and
G. Valdameri, Pharmaceutical Sciences Graduate Program, Laboratory of Cancer Drug Resistance, Federal University of Paraná, Rua Prefeito Lothário Meissner, 632, Jardim Botânico, Curitiba, PR 80210-170, Brazil
Tel: +55(41)33604078
E-mail: gvaldameri@ufpr.br

Diogo Henrique Kita and Gisele Alves de Andrade contributed equally to this article.

(Received 6 August 2021, revised 2 December 2021, accepted 13 December 2021, available online 30 December 2021)

doi:10.1002/1873-3468.14265

Edited by Stuart Ferguson

A promising strategy to overcome multidrug resistance is the use of inhibitors of ABC drug transporters. For this reason, we evaluated the polyoxovanadates (POVs) $[V_{10}O_{28}]^{6-}$ (V_{10}), $[H_6V_{14}O_{38}(PO_4)]^{5-}$ (V_{14}), $[V_{15}O_{36}Cl]^{6-}$ (V_{15}) and $[V_{18}O_{42}I]^{7-}$ (V_{18}) as inhibitors of three major multidrug resistance-linked ABC transporters: P-glycoprotein (P-gp), ABCG2 and MRP1. All of the POVs selectively inhibited P-gp. V_{10} and V_{18} were the two most promising compounds, with IC_{50} values of transport inhibition of 25.4 and 22.7 μM, respectively. Both compounds inhibited P-gp ATPase activity, with the same IC_{50} value of 1.26 μM. V_{10} and V_{18} triggered different conformational changes in the P-gp protein with time-dependent inhibition, which was confirmed using the synthesized salt of V_{10} with rhodamine B, RhoB-V_{10}. The hydrophilic nature of POVs supports the hypothesis that these compounds target an unusual ligand-binding site, opening new possibilities in the development of potent modulators of ABC transporters.

Keywords: ABC transporters; cancer; inhibitors; multidrug resistance; P-glycoprotein; polyoxovanadates

Abbreviations
ABC, ATP-binding cassette; ADP, adenosine diphosphate; CAN, Ca^{2+}-activated, non-selective; CHO, Chinese hamster ovary; DMEM, Dubecco's modified eagle medium; I_{MAX}, maximal inhibition percentage; MDR, multidrug resistance; NBD, nucleotide-binding domain; NMDG, *N*-methyl-D-glucamine; P-gp, P-glycoprotein; POM, polyoxometalate; POT, polyoxotungstates; POV, polyoxovanadate; Rho, rhodamine; RhoB, Rhodamine B; TGA, thermogravimetric analysis; TMD, transmembrane domain.

ATP-binding cassette (ABC) proteins constitute one of the largest, most diverse and ubiquitous protein superfamilies [1]. These transmembrane efflux proteins are involved in the unidirectional transport of a variety of molecules across biological membranes [2]. There are 48 ABC proteins present in humans that function as pumps, effluxing substrates from cells by using the ATP-binding energy [3]. In addition to an important detoxifying action, ABC transporters also have a prominent role in conferring multidrug resistance (MDR) to cancer cells [4,5], attenuating their response to chemotherapy. Among the main ABC transporters overexpressed in resistant cancer cells, ABCB1/P-gp (P-glycoprotein, MDR1) was the first identified [6], followed by ABCC1/MRP1 (multidrug resistance protein 1) [7] and ABCG2/ABCP, which is abundant in the placenta [8], BCRP (breast cancer resistance protein) [9], and MXR (mitoxantrone resistance protein) [10].

Despite the availability of structural information on P-gp and intense research on the molecular mechanism of drug binding and transport, the coupling of the conformational transitions of transmembrane domains (TMDs) to the ATPase cycle is not fully understood [11]. Since P-gp is a validated therapeutic target, the discovery of new inhibitors that bind its different sites is a valuable strategy to better understand inhibition mechanisms. Although three generations of P-gp inhibitors have been developed and tested clinically, most clinical trials have had minimal success [12]. In this context, new approaches are needed to overcome MDR and improve the efficacy of chemotherapeutic treatments.

Polyoxometalates (POMs) are a class of metal (W, Mo, Nb and V) oxides exhibiting a wide variety of structures [13]. Polyoxovanadates (POVs), a subclass of POMs, have emerging biomedical applications including antidiabetic, antibacterial, antiprotozoal, antiviral and anticancer activities [14]. Among them, decavanadate, $[V_{10}O_{28}]^{6-}$ or $\mathbf{V_{10}}$, which deserves special attention due to its anticancer activities [13,15,16]. Decavanadate is well known for interacting with phosphate-dependent proteins such as ion pumps, ATPases and actin [17-19]. It is capable of binding various E1-E2 ATPases, especially Ca^{2+}-ATPase, having high affinity for all conformations [20]. Regarding ABC ATPases, $\mathbf{V_{10}}$ has shown an inhibitory role against the *Escherichia coli* DNA-repairing protein MutS [17]. Moreover, decavanadate has consistently shown higher affinity for these proteins as compared to orthovanadate, $[VO_4]^{3-}$ or V_1, thus stimulating further studies on this polynuclear anion's binding mechanism and inferring the chemical species involved. One additional advantage of V_{10} is its stability in acidic media and its kinetic stability under physiological conditions, wherein once V_{10} is formed, it is prone to be stabilized by cytosolic and membrane proteins, which extends its half-life to hours [21].

Although there is still much work to be done with POVs, this class shows potential to be applied in oncolytic virus therapy, against viral and drug-resistant bacterial infections, as well as in the chemotherapy of solid tumours [14]. Moreover, the two most important oxidation states of vanadium (V^{IV} and V^{V}) accessible in biological conditions are present in mixed-valence polyoxovanadates (MV-POV). Over the past decade, many studies have addressed the effect of V_{10}, and more recently MV-POVs, assessing their interaction with lipids [22], reverse micelles [23] and cell membranes, indirectly activating a specific G Protein-Coupled Receptor [24]. In spite of numerous reports on $\mathbf{V_{10}}$ and higher-nuclearity POVs in their interaction with a variety of biological targets [13,24] and as anticancer drugs [13,25], no study has been carried out targeting ABC transporters associated with MDR. The present work evaluated the ABC transporter inhibitory activity of VO_4^{3-} and four POVs, namely decavanadate ($\mathbf{V_{10}}$) and three mixed-valence POVs, $\mathbf{V_{14}}$, $\mathbf{V_{15}}$ and $\mathbf{V_{18}}$ (Fig. 1). Additionally, a decavanadate derivative containing Rhodamine B as a counterion was synthesized and characterized to investigate the intracellular accumulation of $\mathbf{V_{10}}$. We also identified and characterized the biochemical mechanism of action of some POVs that specifically inhibit P-gp activity.

Results

POVs are specific P-gp inhibitors

To evaluate the ability of POVs to inhibit ABC transporter activity, a live-cell efflux assay was used, which allows the study of protein-drug binding and transport in a native cell environment. For this approach, cells stably transfected with each of the three most important ABC transporters implicated in cancer resistance were used. First, the effect of decavanadate ($\mathbf{V_{10}}$) on P-gp activity was compared with the effect of sodium orthovanadate ($\mathbf{V_1}$), which is routinely used to inhibit the ATPase activity of ABC transporters in membrane preparations. As shown in Fig. 2A, $\mathbf{V_1}$ was not very effective at inhibiting P-gp activity, with only weak inhibitory activity at the highest concentration, 50.0 μM (Fig. 2A). In sharp contrast, P-gp activity was almost completely inhibited by $\mathbf{V_{10}}$ at 50.0 μM (Fig. 2A). This result confirms the pharmacological potential of polyoxovanadate salts.

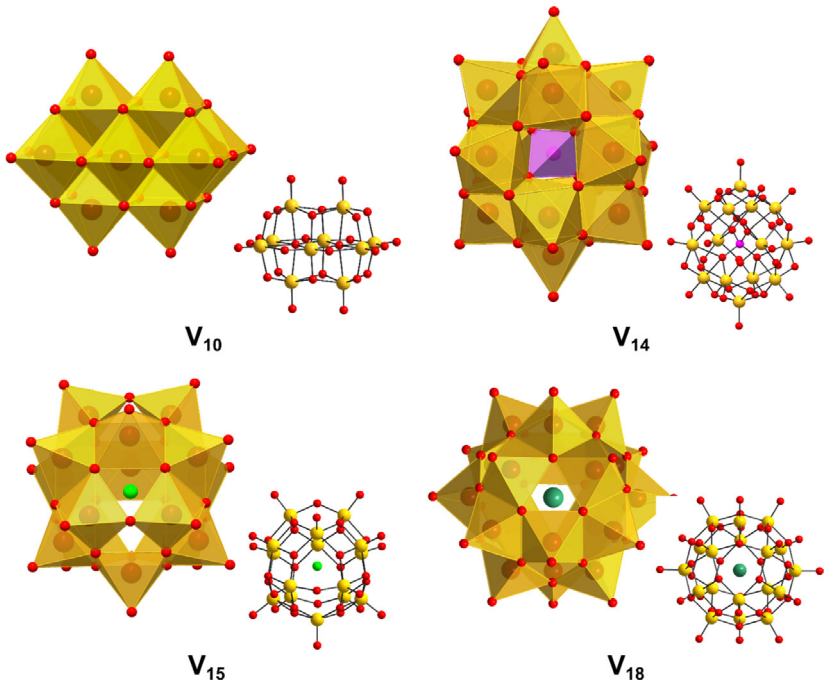

Fig. 1. Polyoxovanadates used in the present work as potential ABC-transporter inhibitors: $[V_{10}O_{28}]^{6-}$ (**V_{10}**), $[H_6V_{14}O_{38}(PO_4)]^{4-}$ (**V_{14}**), $[V_{15}O_{36}Cl]^{6-}$ (**V_{15}**) and $[V_{18}O_{42}I]^{8-}$ (**V_{18}**) [24-26].

Considering that the nucleotide-binding domains (NBDs) are highly conserved among ABC proteins [26], and that decavanadate interacts with the Walker A motif [17], the effect of **V_{10}** was also evaluated on ABCG2 and MRP1 activity. Interestingly, **V_{10}** failed to inhibit the transport activity of ABCG2 and MRP1, even at high concentrations such as 50.0 μM (Fig. 2A). The same was observed to **V_1** (Fig. 2A). This result refuted our original hypothesis that targeting the NBDs could lead to the development of pan-inhibitors of ABC transporters to be used in cell-based models; on the other hand, a novel class of compounds was identified as potential specific P-gp inhibitors.

To elucidate the relationship between structural aspects of POVs and P-gp inhibition, three mixed-valence POVs (**V_{14}**, **V_{15}** and **V_{18}**) were also evaluated. As shown in Fig. 2B, all three compounds selectively inhibited P-gp activity, since no significant effect was observed on ABCG2 or MRP1. Various concentrations of the POVs up to 250 μM were used to identify the IC_{50} values for inhibition (Table 1, Fig. 3A and Fig. S1). No clear correlation was observed between the number of vanadium atoms and the potency of P-glycoprotein inhibition, since **V_{10}** and **V_{18}** were the two best inhibitors, showing similar IC_{50} values (Table 1). In addition, it is relevant that these compounds completely inhibit P-gp, as evidenced by the I_{MAX} values (Table 1).

Mechanism of V_{10} and V_{18} P-gp inhibition

To obtain estimates of the constants characterizing inhibition of P-gp, P-gp activity was measured at several substrate (Rhodamine 123) concentrations, with fixed concentrations (0.0, 10.0, 25.0 and 50.0 μM) of **V_{10}** or **V_{18}**. A mathematical model for estimation of the effective inhibition constants of the polyoxovanadate inhibitors was developed (see Supporting information). The apparent specificity constant of P-gp was affected by these POVs, with inhibition constants of 8.6 μM for **V_{10}** and 5.4 μM for **V_{18}** (Fig. 3B,C).

The intrinsic cytotoxicity of **V_{10}** and **V_{18}** was initially evaluated with respect to NIH3T3 wild-type cells. Both POVs showed IG_{50} values (compound concentrations giving a half-maximal cell viability) of approximately 6 μM (Fig. 4A). Since cross-resistance to the drug can be investigated with compounds that produce a quantifiable cytotoxic effect, an additional cell viability assay was performed to compare the cytotoxic effects of **V_{10}** and **V_{18}** on NIH3T3 wild-type cells and transfected NIH3T3 cells overexpressing P-gp. As shown in Fig. 4A, **V_{10}** and **V_{18}** exhibited the same cytotoxic pattern in both cell lines, indicating no apparent cross-resistance, suggesting that these POVs are not transported by P-gp.

To evaluate the ATPase activity of P-gp, membranes were prepared from baculovirus-infected Sf9 insect cells transfected with the human *ABCB1* gene. As

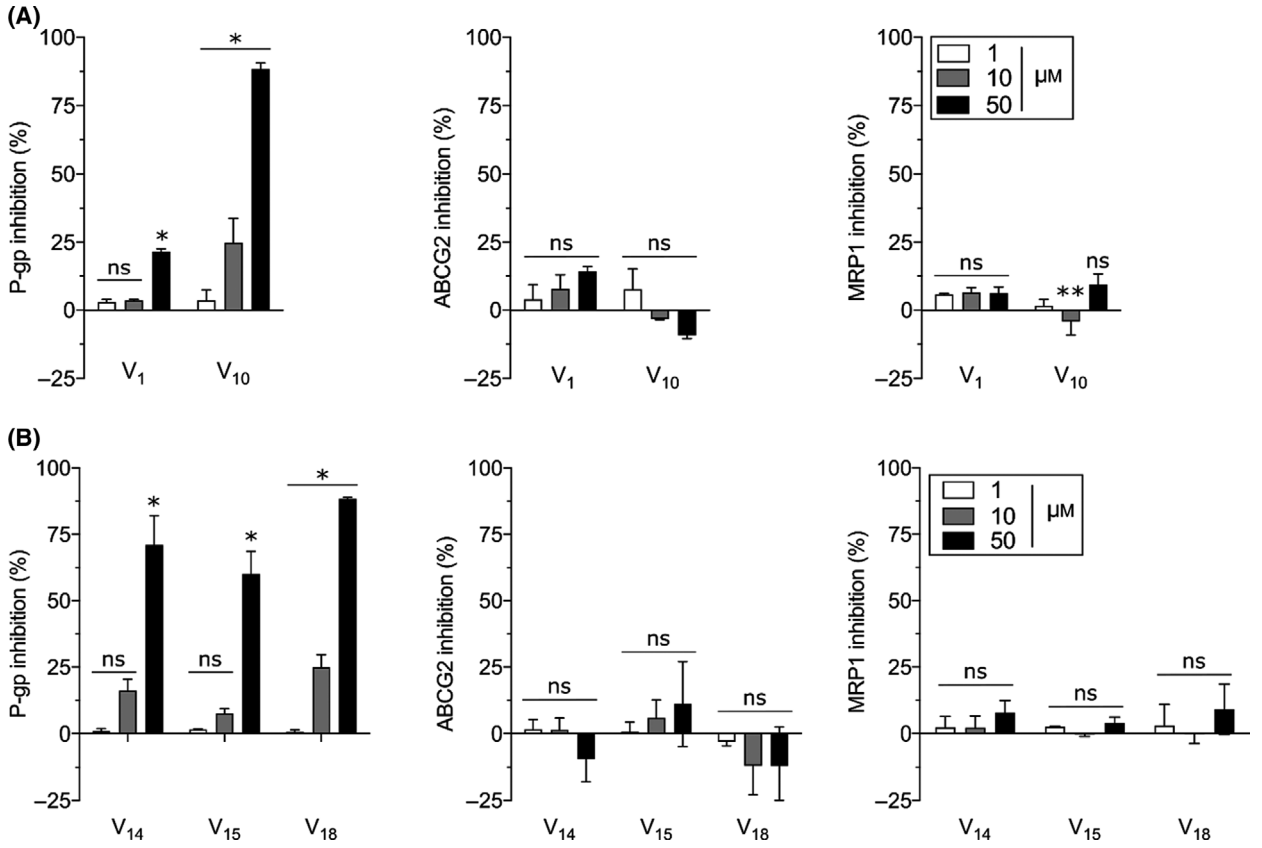

Fig. 2. Inhibition of the transport function of P-gp, ABCG2 and MRP1 by selected vanadate compounds. The inhibition of P-gp-mediated efflux was assayed in stably transfected NIH3T3-P-gp cells using 5.0 μM of Rhodamine 123 as substrate and 1.0 μM of GF120918 as reference inhibitor. The inhibition of ABCG2-mediated efflux was assayed in stably transfected HEK293-ABCG2 cells using 5.0 μM of Mitoxantrone as substrate and 1.0 μM of Ko143 as reference inhibitor. The inhibition of MRP1-mediated efflux was assayed in stably transfected BHK21-MRP1 cells using 0.20 μM of Calcein-AM as substrate and 30.0 μM of Verapamil as reference inhibitor. (A) Effect of $\mathbf{V_1}$ and $\mathbf{V_{10}}$. (B) Effect of $\mathbf{V_{14}}$, $\mathbf{V_{15}}$ and $\mathbf{V_{18}}$. Data are the mean ± SD of three independent experiments. Ns – non significant, *P* value ($P < 0.001$) post-test: Tukey HSD. Statistical analysis was performed by Statistica software (StatSoft, Inc. (2012). Electronic Statistics Textbook. Tulsa, OK: StatSoft, Palo Alto, CA, USA).

Table 1. Inhibition of P-gp-mediated efflux of substrate by POVs. The inhibition of P-gp-mediated efflux was assayed by flow cytometry using stably transfected NIH3T3-P-gp cells and 5.0 μM of Rhodamine 123 as substrate and 1.0 μM of GF120918 as reference inhibitor (100% of inhibition). The affinity of inhibitor interaction was expressed as IC_{50} values (compound concentration giving a half-maximal inhibition). The maximal inhibition percentage (I_{MAX}) was determined by IC_{50} fitted curves.

Compound	IC_{50} μM ± SD	I_{MAX} μM ± SD
$\mathbf{V_{10}}$	25.4 ± 7.9	101.6 ± 9.6
$\mathbf{V_{14}}$	35.6 ± 8.3	107.9 ± 8.1
$\mathbf{V_{15}}$	58.8 ± 16.9	107.2 ± 11.4
$\mathbf{V_{18}}$	22.7 ± 3.6	109.5 ± 5.4

shown in Fig. 4B, $\mathbf{V_{10}}$ and $\mathbf{V_{18}}$ inhibited the ATPase activity of P-gp. Additionally, the effect of $\mathbf{V_{10}}$ and $\mathbf{V_{18}}$ was investigated on membranes prepared from baculovirus-infected Sf9 insect cells transfected with the human *ABCG2* gene. Surprisingly, the ATPase activity of ABCG2 was also inhibited at high concentrations (Fig. 4B). As shown in Table 2, $\mathbf{V_{10}}$ and $\mathbf{V_{18}}$ showed the same IC_{50} value for inhibition, 1.26 μM, for the ATPase activity of P-gp. In contrast, a 10-fold lower affinity for ABCG2 was observed (IC_{50} values of 9.38 μM for $\mathbf{V_{10}}$ and 11.23 μM for $\mathbf{V_{18}}$). This significant difference suggests that the conserved regions of NBDs are not the unique target of POVs, and supports the selective inhibition of P-gp transport activity.

Conformational changes triggered by ligands can be explored by flow cytometry using antibodies that recognize extracellular regions of TMDs. Exposure of NIH3T3-P-gp cells to the substrate Rhodamine 123 did not change the conformational antibody binding (Fig. 4C,D). However, the reference inhibitor GF120918 (Elacridar) increased the antibody binding, suggesting an important allosteric rearrangement of

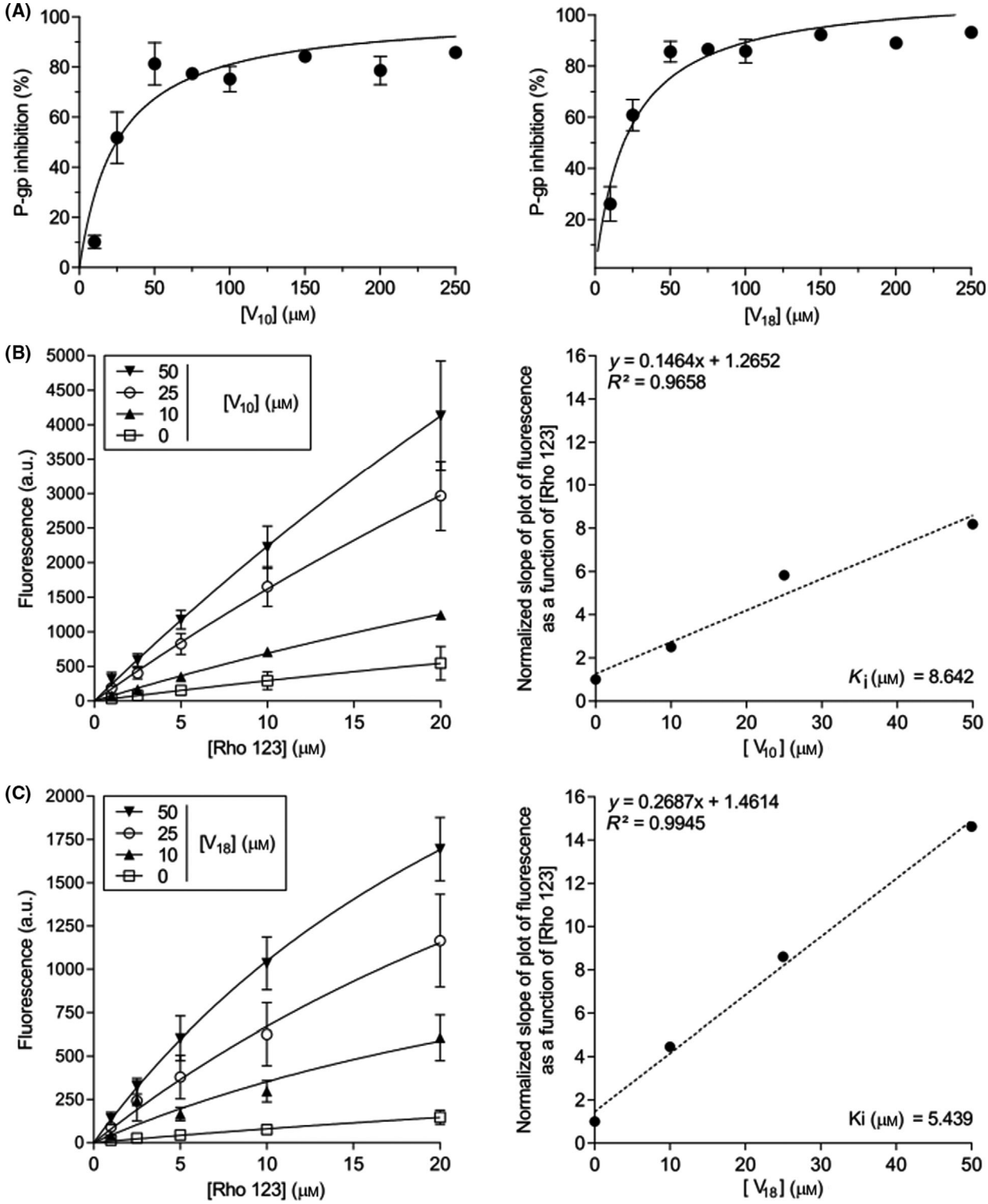

Fig. 3. Nature of inhibition by POVs. The inhibition of P-gp-mediated efflux was assayed by flow cytometry using stably transfected NIH3T3-P-gp cells using 5.0 μM of Rhodamine 123 as substrate and 1.0 μM of GF120918 as reference inhibitor. (A) Representative IC_{50} curves of **V_{10}** and **V_{18}** inhibitors. (B) Intracellular accumulation of Rhodamine 123 promoted by **V_{10}** and kinetic parameters. (C) Intracellular accumulation of Rhodamine 123 caused by **V_{18}** and kinetic parameters. The K_M and the V_{max} values were determined using the GRAPHPRISM software (GraphPad Software, San Diego, CA, USA).

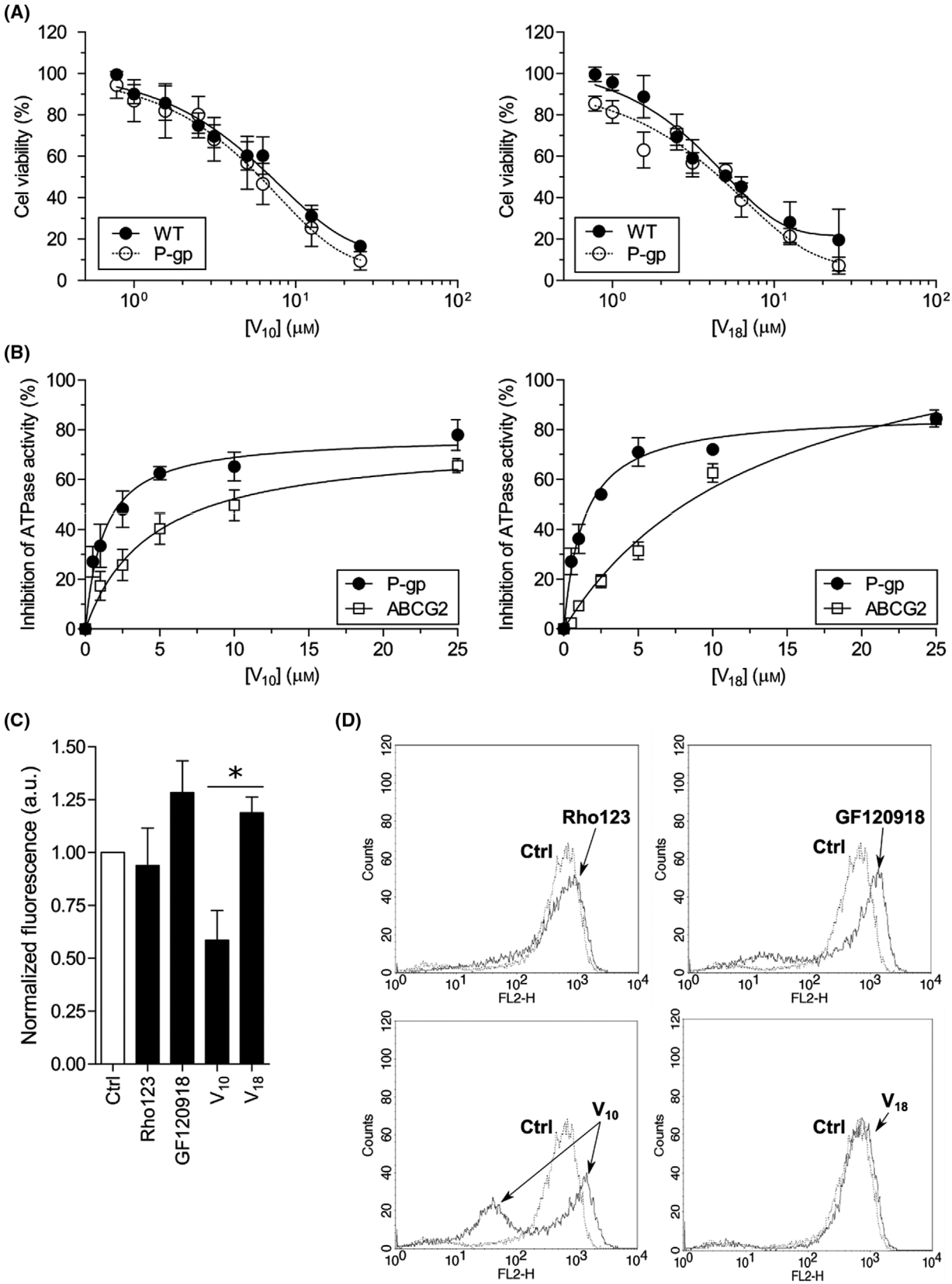

Fig. 4. Effect of $\mathbf{V_{10}}$ and $\mathbf{V_{18}}$ on cell viability, ATPase activity and conformational 17F9 antibody binding. (A) Cell viability was assayed by MTT in NIH-3T3 wild-type and stably transfected NIH3T3-P-gp cells. (B) Effect of compounds on basal P-gp and ABCG2 ATPase activity. (C) Effect of compounds $\mathbf{V_{10}}$ and $\mathbf{V_{18}}$ on conformational 17F9 antibody binding. Data are the mean ± SD of two independent experiments. Statistical analysis showed a significant difference between $\mathbf{V_{10}}$ and $\mathbf{V_{18}}$ ($P = 0.033$). As compared to Rho123, they did not show significant difference ($P > 0.05$). Post-test: Tukey. (D) Histogram showing the effect of compounds $\mathbf{V_{10}}$ and $\mathbf{V_{18}}$ on conformational 17F9 antibody binding.

Table 2. Inhibition of the ATPase activity of P-gp and ABCG2 by POVs. Effect of $\mathbf{V_{10}}$ and $\mathbf{V_{18}}$ inhibitors on the ATPase activity of P-gp and ABCG2. The vanadate-sensitive ATPase activity of P-gp and ABCG2 was measured using the total membranes of High-Five insect cells expressing each transporter. The IC_{50} (concentration required to achieve 50% of inhibition) is given as the concentration ± SD (μM) of three independent experiments in duplicate.

ABC transporter	Compound	IC_{50} μM ± SD
P-gp	$\mathbf{V_{10}}$	1.26 ± 0.31
	$\mathbf{V_{18}}$	1.26 ± 0.22
ABCG2	$\mathbf{V_{10}}$	9.38 ± 0.99
	$\mathbf{V_{18}}$	11.23 ± 1.48

TMDs in the presence of that inhibitor. $\mathbf{V_{10}}$ and $\mathbf{V_{18}}$ had very different effects. While $\mathbf{V_{18}}$ did not affect the antibody binding, $\mathbf{V_{10}}$ triggered an unusual effect, as evidenced by two distinct cell populations seen in the histogram, one showing reduced antibody binding and a second cell population with increased antibody binding (Fig. 4C,D). The significant differences between the effects produced by $\mathbf{V_{10}}$ and $\mathbf{V_{18}}$ suggest that these POVs have different binding sites on P-gp.

Considering the large size of the POVs, a time-course drug-uptake experiment was performed to measure P-gp inhibition. Cells were exposed to $\mathbf{V_{10}}$ and $\mathbf{V_{18}}$ for three different periods of time (30 min, 1 and 3 h). Exposure for 30 min corresponds to the same protocol used for all experiments described in this work. As shown in Fig. 5A, increasing the exposure time to both POVs up to 3 h significantly increased the percentage of P-gp inhibition. This effect can be easily observed with 10.0 μM $\mathbf{V_{10}}$, which increased the inhibition from 29% to 88%. This effect suggests that these compounds need more than 30 min to enter the cell, probably due to their low hydrophobicity, a feature commonly observed for P-gp inhibitors. Another possibility may be related with the breakage of V_{10} in the culture medium to form oligomers of lower nuclearity in the course of the experiment (See speciation studies below).

To confirm that $\mathbf{V_{10}}$ and $\mathbf{V_{18}}$ are not transported by P-gp, the same approach (a time-course experiment) was used, but the monolayers of cells were washed twice with PBS before incubation with the substrate. Our results showed that the degree of inhibition was the same with or without washing to remove the $\mathbf{V_{10}}$ and $\mathbf{V_{18}}$ inhibitors (Fig. 5B), confirming the results shown in Fig. 4A for the cell viability assay.

Synthesis and characterization of $(RhoBH)_4[H_2V_{10}O_{28}]\cdot 2RhoB\cdot 14H_2O$ (RhoB-V_{10})

It was recently demonstrated that POVs are able to interact with the lipidic membranes of CHO cells [24], an initial step to their possible internalization. To further investigate the potential of POVs to cross cell membranes (see also the next section), a decavanadate complex with the fluorescent dye Rhodamine B (**RhoB**) was synthesized to evaluate the intracellular uptake of $\mathbf{V_{10}}$ by flow cytometry. **RhoB** was chosen because of its ability to cross cell membranes, and, unlike Rhodamine 123 (Rho123) and mitoxantrone, it is not transported by P-gp [27] (see Fig. 7).

The single-crystal X-ray diffraction analysis of $(RhoBH)_4[H_2V_{10}O_{28}]\cdot 2RhoB\cdot 14H_2O$, **RhoB-$V_{10}$**, showed that the compound crystalizes in the triclinic $P\bar{1}$ system. The asymmetric unit consists of two protonated rhodamine molecules ($RhoBH^+$), one neutral zwitterionic species (RhoB), one half of a doubly protonated decavanadate anion [28] and seven water molecules. The other half of the structure builds itself through an inversion centre located in the middle of the polyoxoanion (Fig. 6 and Fig. S2).

The decavanadate anion displays bond lengths and angles in accordance with other V_{10} data reported in the literature [28] (Table 3). As for the Rhodamine B moieties, during the reaction, the pH was adjusted to 4, favouring the cation *vs.* the zwitterionic form (pKa = 3.7, Fig. S3) [29] as confirmed by X-ray diffraction analysis. In the neutral species, the carboxyl group resonance can be inferred by the similar carbon–oxygen bond lengths (O(25)–C(27) = 1.228(5) Å, O(26)–C(27) = 1.273(5) Å, see Table 3). In the $RhoBH^+$ cations, on the other hand, these bond lengths are rather different (O(91)–C(93) = 1.197(5) Å, O(92)–C(93) = 1.314(5) Å, Table 3).

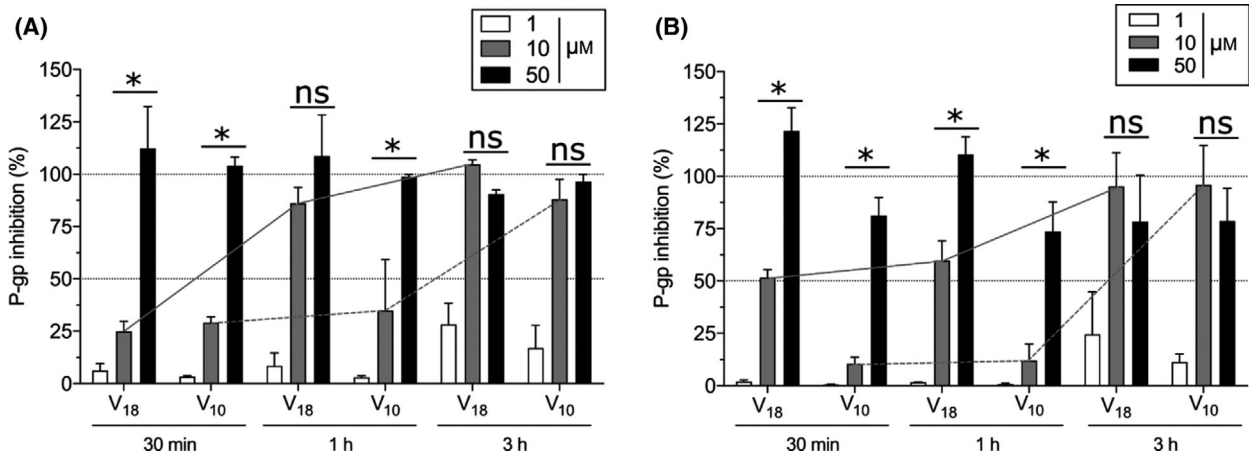

Fig. 5. Time course of the incubation and washing assay. The inhibition of P-gp-mediated efflux was assayed in stably transfected NIH3T3-P-gp cells using 5.0 μM of Rhodamine 123 as substrate and 1.0 μM of GF120918 as reference inhibitor. (A) Addition of substrate to the culture medium containing the inhibitors. Effect of $\mathbf{V_{10}}$ and $\mathbf{V_{18}}$ after 30 min, 1 and 3 h of exposure. (B) Addition of substrate after washing cells twice with PBS. Data are the mean ± SD of three independent experiments. Compared with T-test, the 10-μM group showed no significant difference after a 1-h incubation ($P > 0.05$) between washed and not washed assays.

Intracellular accumulation of the decavanadate-RhoB complex (RhoB-V_{10})

Figure 7A compares the P-gp-mediated intake of RhoB, Rho123 and Mtx, confirming the lack of transport of Rhodamine B. Based on this information, we investigated the intracellular accumulation of the decavanadate-RhoB complex (**RhoB-V_{10}**) by flow cytometry and confocal microscopy. As presented in Fig. 7B,C, the intracellular accumulation of RhoB alone and **RhoB-V_{10}** was similar. Also, similarly to $\mathbf{V_{10}}$, **RhoB-V_{10}** inhibited the P-gp-mediated efflux of two well-known substrates, Rho123 and mitoxantrone. These results support the hypothesis that POVs such as $\mathbf{V_{10}}$, or one of the possible oligovanadates formed by speciation of the polyoxoanion, can be internalized and then bind their respective targets, in this case P-gp (Fig. 7D).

To further investigate the time-dependent P-gp inhibition by POVs, we performed a time-course experiment to detect the maximal level of fluorescence associated with the entry of **RhoB-V_{10}** in the cells. Figure 8A suggests that internalization slows down after 4 h, reaching a plateau after 6 h of incubation with the modified dye. This supports an association between the time-dependent P-gp inhibition and the time needed for the POVs to reach their highest intracellular concentration.

Speciation studies of POVs in solution

Detailed speciation studies of $\mathbf{V_{10}}$, $\mathbf{V_{14}}$ and $\mathbf{V_{15}}$ in aqueous solution, LB and DMEM media by ^{51}V NMR and Continuous-Wave Electron Paramagnetic Resonance (CW-EPR, X-band, 9.5 GHz) spectroscopies were recently reported by some of the authors [24,30], while V_{18} stability studies have been evaluated only in aqueous solution and in LB medium [31]. The inhibition assays described in this work were performed in DMEM at 37 °C for a maximum of 3 h. To shed light onto the nature of the chemical species present in the culture medium and their stability throughout the experiments described in this work, solutions of **RhoB-V_{10}**, $\mathbf{V_{10}}$ and $\mathbf{V_{18}}$ were analysed by ^{51}V NMR spectroscopy at 0, 1 and 3 h, reflecting inhibition of the P-gp-mediated efflux assay (Fig. 5). Being a MV-POV, $\mathbf{V_{18}}$ was also analysed by EPR spectroscopy to characterize the V^{IV} species. For **RhoB-V_{10}** complex, the ^{51}VNMR analysis was performed (at 0 and 4 h) to bring light to the chemical species present in solution during the intracellular accumulation assay. The speciation studies conducted for this work as well as selected data from previous reports are summarized in Table 4.

RhoB-V_{10} dissolves in dmso, exhibiting NMR signals typical of the decavanadate anion [32]. These signals correspond to the two central vanadium atoms (V_A) at –420 ppm, four equatorial atoms (V_B) at –500 ppm and four capping vanadium atoms (V_C) at –522 ppm (Fig. S6). These chemical shifts correspond to the fully deprotonated $[V_{10}O_{28}]^{6-}$ species, as confirmed particularly by those for V_B and V_C, which are more susceptible to protonation and interaction with the medium [32]. The NMR spectrum does not change

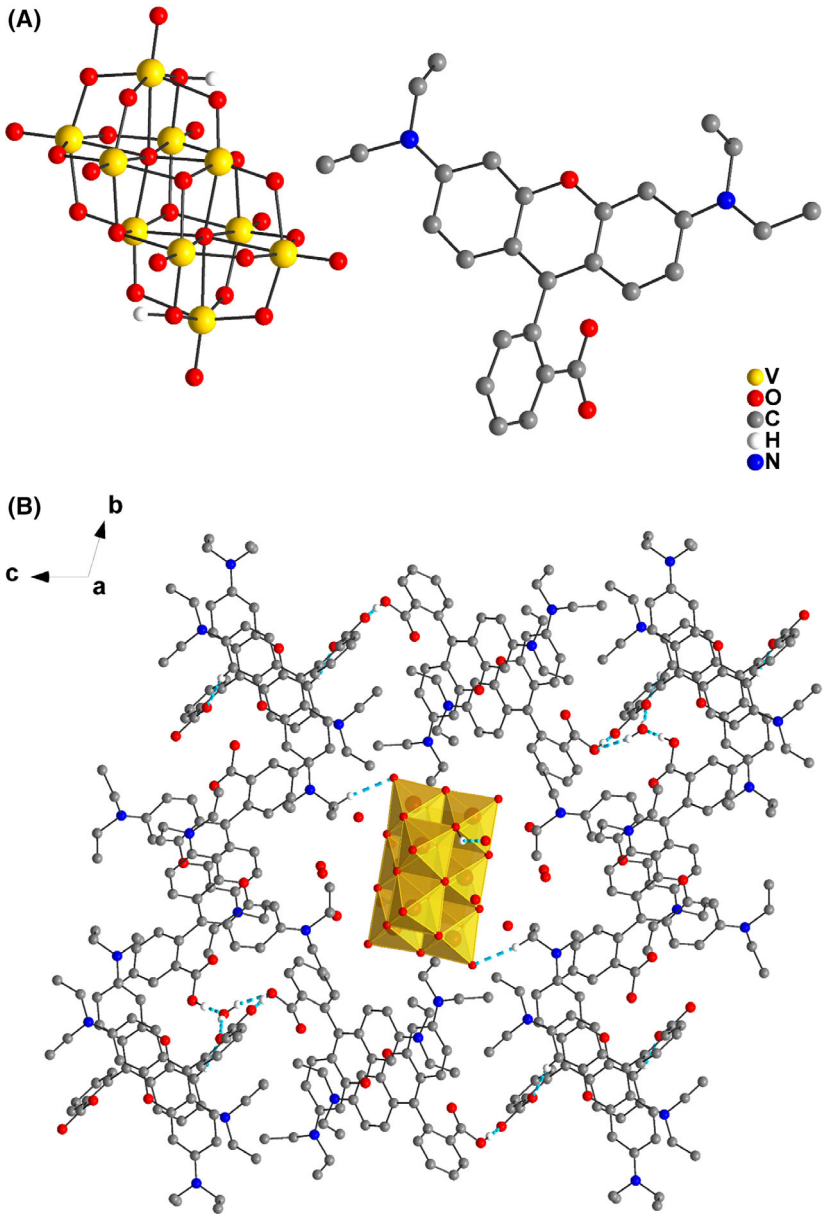

Fig. 6. RhoB-V_{10} structure. (A) Doubly protonated decavanadate anion and the crystallographically independent Rhodamine B zwitterion in the structure of $(RhoBH)_4[H_2V_{10}O_{28}]\cdot 2RhoB\cdot 14H_2O$ (**RhoB-V_{10}**). Hydrogen atoms have been omitted for clarity, except for those belonging to the decavanadate anion. (B) Unit cell of **RhoB-V_{10}** showing the decavanadate anion positioned in the middle of the cell and surrounded by the Rhodamine B moieties. Hydrogen atoms have been omitted for clarity, except for those that participate in hydrogen bonds, which are represented in cyan and are further described in Table S2.

even after incubation for 4 h at 37 °C, indicating that the polyoxovanadate structure in **RhoB-V_{10}** remains intact in dmso.

A freshly prepared dmso solution of **RhoB-V_{10}** diluted in DMEM culture medium (1 : 9) produced a spectrum containing the three signals of monoprotonated $[HV_{10}O_{28}]^{5-}$ at –422, –497 and –513 ppm (Fig. 8B). Additional signals were observed at –573 and –579 ppm, assigned to $[HV_2O_7]^{3-}$ (V_2) and $[V_4O_{12}]^{4-}$ (V_4), respectively, probably generated from the fragmentation of the polyoxoanion [32]. The signal centred at −560 ppm is assigned to V_1 and a vanadate-phosphate binuclear structure (PV, $HVPO_7^{3-}$) expected to exist in a phosphate-rich medium such as DMEM [33].

The above results were not completely unexpected, since the DMEM medium (pH 7.2–7.4) falls in the pH range well-known to establish a delicate equilibrium involving multiple vanadate oligomers [32]. Accordingly, the ^{51}V NMR signals for the low-nuclearity species (V_1, V_2 and V_4) increase in intensity during the time course of the experiment (4 h), whereas the signals related to **V_{10}** diminish (Fig. 8B). These results indicate that more than one vanadium species could be responsible for the biological effects of **RhoB-V_{10}**. Nonetheless, the appearance of such mono- and

Table 3. Selected bond distances and angles in the structure of $(RhoBH)_4[H_2V_{10}O_{28}]\cdot 2RhoB\cdot 14H_2O$ (**RhoB-V_{10}**). CCDC deposition number: 2120954. Although the crystallographic disorder involving the water molecules prevented their hydrogen atoms to be located on the difference map, results of elemental, thermogravimetric and spectroscopic analyses confirm the formulation $(RhoBH)_4[H_2V_{10}O_{28}]\cdot 2RhoB\cdot 14H_2O$ proposed for **RhoB-V_{10}**. These results are presented in Synthesis and characterization of $(RhoBH)_4[H_2V_{10}O_{28}]\cdot 2RhoB\cdot 14H_2O$ (RhoB-V_{10}) and as Supplementary Information (Figs S4 and S5, Table S3).

Selected bond lengths (Å)			
V(1)–O(1)	1.603(3)	V(4)–O(4)#1	2.069(3)
V(2)–O(5)	1.594(3)	V(1)–O(13)#1	1.977(3)
V(5)–O(7)	1.600(3)	V(3)–O(13)	1.902(3)
V(4)–O(14)	1.595(3)	V(4)–O(13)	1.960(3)
V(1)–O(2)	1.794(3)	V(1)–O(9)#1	2.290(3)
V(2)–O(2)	1.860(3)	V(2)–O(9)#1	2.308(2)
V(1)–O(3)	1.843(3)	V(3)–O(9)	2.062(3)
V(5)–O(3)	1.841(3)	V(3)–O(9)#1	2.129(2)
V(2)–O(6)	1.819(3)	V(4)–O(9)#1	2.246(3)
V(5)–O(6)	1.828(3)	V(5)–O(9)#1	2.312(3)
V(3)–O(8)	1.677(3)	C(68)–N(71)	1.446(7)
V(5)–O(8)	2.010(3)	N(71)–C(72)	1.345(5)
V(2)–O(10)#1	2.036(3)	C(93)–C(94)	1.492(6)
V(3)–O(10)	1.688(3)	O(91)–C(93)	1.197(5)
V(4)–O(12)	1.743(3)	O(92)–C(93)	1.314(5)
V(5)–O(12)	1.947(3)	C(2)–N(5)	1.455(6)
V(2)–O(11)	1.913(3)	N(5)–C(6)	1.348(5)
V(4)–O(11)	1.895(3)	C(27)–C(28)	1.503(6)
V(1)–O(4)	2.036(3)	O(25)–C(27)	1.228(5)
V(3)–O(4)	1.970(3)	O(26)–C(27)	1.273(5)
Selected bond angles (°)			
O(1)–V(1)–O(2)	104.26(15)	V(3)–O(9)–V(3)#1	101.25(10)
O(2)–V(1)–O(13)#1	91.92(12)	V(3)–O(9)–V(5)#1	171.02(13)
O(2)–V(1)–O(4)	154.88(12)	V(2)#1–O(9)–V(5)#1	83.14(8)
O(1)–V(1)–O(9)#1	174.13(14)	C(6)–N(5)–C(2)	120.9(4)
O(11)–V(2)–O(10)#1	83.66(12)	O(26)–C(27)–C(28)	115.3(4)
O(10)–V(3)–O(13)	98.20(13)	C(72)–N(71)–C(68)	122.0(4)
O(13)–V(4)–O(9)#1	76.91(10)	C(93)–O(92)–H(92)	120(3)
O(7)–V(5)–O(9)#1	174.46(13)	O(91)–C(93)–C(94)	122.8(4)
V(1)–O(2)–V(2)	115.64(14)	O(92)–C(93)–C(94)	113.7(4)
V(1)–O(4)–V(4)#1	97.57(12)		

oligomeric species does not seem to interfere with the inhibition of P-gp, suggesting that the polyoxoanion binds the protein irreversibly.

Unlike **RhoB-V_{10}**, **NaV_{10}** and **V_{18}** are highly soluble in water, and the ^{51}V NMR spectra were registered directly from freshly prepared solutions in the DMEM culture medium, and also after 1 and 3 h of incubation at 37 °C. The spectrum recorded for the freshly prepared sample of **V_{10}** (Fig. 9A) showed signals at –420, –495 and –512 ppm assigned to V_A, V_B and V_C of $[V_{10}O_{28}]^{6-}$, along with signals for V_1 (–558 ppm), V_2 (–572 ppm) and V_4 (–577 ppm), evidencing fragmentation of V_{10} [32]. After incubation at 37 °C for 1 h, the intensity of the V_{10} signals diminished significantly, and it was no longer possible to identify the V_A signal. Also, there was an increase in the signal from the V_4 species, and a signal pertaining to the $[V_5O_{15}]^{5-}$ species (V_5) appeared at –585 ppm. After a 3-h incubation, the V_{10} signals disappeared completely, as shown in the insert in Fig. 9A. As there was a sharp increase in the intensity of the V_4 signal, it became the predominant species. Taking into account the lower stability of **V_{10}** compared to that of **RhoB-V_{10}**, it is still tricky to state whether the observed effects are related to the presence of both **V_{10}** and **V_4**, or whether they could be possibly attributed to only one of them.

V_{18}, in turn, is a paramagnetic POV whose aqueous and DMEM solutions were also submitted to Continuous-Wave Electron Paramagnetic Resonance (CW-EPR, X-band, 9.5 GHz) analysis at 77 K to look for additional stability information. The EPR spectrum of a freshly prepared solution (1.0 mM) of **V_{18}** in pure water presented only a broad band, as expected for the mixed-valence polynuclear aggregate, with $g = 1.9674$ and $\Delta_{p\text{-}p} = 33.13$ mT (data not shown). Only a very weak signal of V_1 was observed in the ^{51}V NMR spectrum (Fig. S7), suggesting that the aggregate is fairly stable in aqueous solution. On the other hand, the EPR spectrum of **V_{18}** in the culture medium exhibited a low-intensity signal of a mononuclear species (Fig. 8C), and its intensity increased up to 3 h of analysis, indicating some breakage of the polyoxovanadate to give a mononuclear oxovanadium(IV) species. This signal differs from the one given by the $[VO(OH_2)_5]^{2+}$ species that is known to predominate in aqueous solutions of vanadium(IV) [34], suggesting a possible reaction of the released mononuclear species with one of the coordinating components of the medium. Such fragmentation of **V_{18}** is also observed in the ^{51}V NMR spectrum (Fig. 8B) through the presence of low intensity signals. Across the whole length of the experiment, only three signals were seen in the spectra: the first, at –557 ppm, refers to V_1; the second, at –571 ppm, corresponds to V_2; and the third, at –577 ppm, refers to V_4 [32].

Discussion

Biological effects

Human ABC transporters are categorized either as full transporters containing at least two transmembrane domains (TMDs) and two nucleotide-binding domains (NBDs), or as half transporters containing one TMD and one NBD, which form functional homo or heterodimers [35]. The TMDs contain from 6 to 12 membrane-spanning α-helices that interact with their

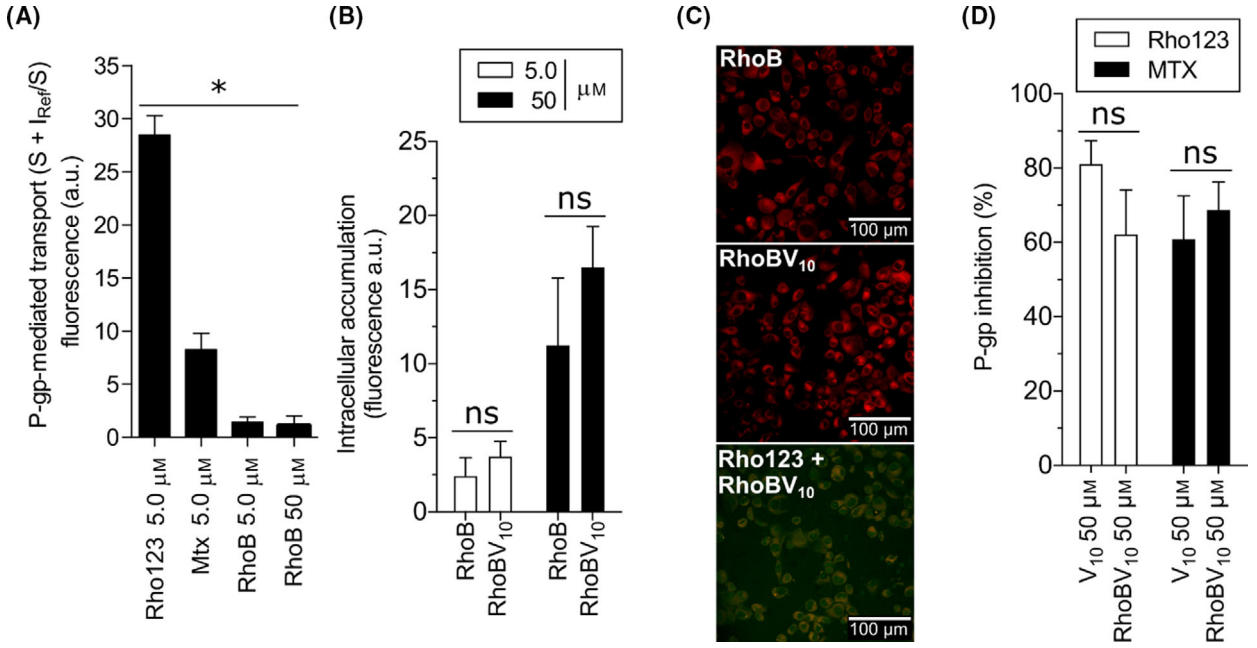

Fig. 7. Internalization and activity of **RhoB-V_{10}**. (A) Transport of fluorescent dyes by P-gp. Statistical analysis showed significant difference between Rho123, Mtx and RhoB ($P < 0.001$). (B) Intracellular accumulation of Rhodamine B (**RhoB**) and **RhoB-V_{10}** in NIH3T3 wild-type cells quantified by flow cytometry. **RhoB** and **RhoB-V_{10}** showed no statistical difference ($P > 0.05$) (C) Confocal images of stably transfected NIH3T3-P-gp cells using 5.0 µM of **RhoB**, 5.0 µM of **RhoB-V_{10}** and concomitant incubation of 5.0 µM of **Rho123** and 50.0 µM of **RhoB-V_{10}**. (D) Effect of **V_{10}** and **RhoB-V_{10}** on P-gp activity. P-gp-mediated efflux was assayed in stably transfected NIH3T3-P-gp cells using 5.0 µM of Rhodamine 123 and Mitoxantrone (mtx) as substrates and 1.0 µM of GF120918 as reference inhibitor. Statistical analysis showed no significant difference between substrates ($P > 0.05$). Data are the mean ± SD of three independent experiments.

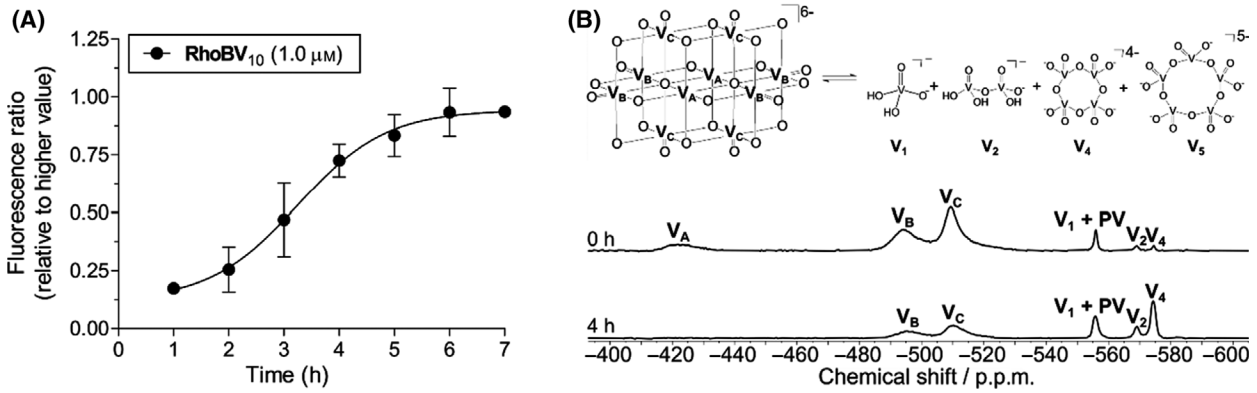

Fig. 8. Intracellular accumulation of **RhoB-V_{10}** and ^{51}V NMR spectra (A) Intracellular accumulation of **RhoB-V_{10}** in NIH3T3 wild-type cells quantified by flow cytometry. (B) ^{51}V NMR spectra recorded at 1.0 mM at pH 7.2–7.4 for **RhoB-V_{10}** in dmso/DMEM (1 : 9). The spectrum at 0 h was generated from a freshly prepared solution and the spectrum at 4 h was produced from the solution incubated at 37 °C. The low nuclearity vanadium(V) species identified in the spectra were 'V_1' = $H_2VO_4^-$; 'PV' = $HVPO_7^{3-}$; 'V_2' = $H_2V_2O_7^{2-}$ and 'V_4' = $V_4O_{12}^{4-}$.

substrates and inhibitors based on their hydrophobic properties. The highly conserved NBDs are located in the cytoplasm [26]. Considering that the ATPase activity of several ABC transporters is inhibited by phosphate-mimicking anions such as the orthovanadate routinely used in ATPase assays [11,36], we hypothesized that compounds targeting the NBDs could be used as ABC transporter pan-inhibitors. Vanadium complexes, mostly decavanadate, have exhibited several biological properties in cell-based models, and have been described to bind, with high affinity, to the inorganic phosphate (P_i)-binding site of

Table 4. Detectable vanadium-containing species in **V_{10}** [24], **RhoB-V_{10}** and **V_{18}** [31] in solutions with an initial concentration of 1.0 mmol·L^{-1} of each polyoxovanadate, using ^{51}V NMR and EPR spectroscopies.

	Polyoxovanadate		
Condition	**V_{10}**	**RhoB-V_{10}**	**V_{18}**
H_2O solution[a,b]	V_{10}	–	MV-POV[c], $V^{IV}O$[c], V_1
dmso solution[d]	–	V_{10}	–
DMEM (t = 0 h)[d]	V_{10}, V_1+PV, V_2, V_4	V_{10}, V_1+PV, V_2, V_4	MV-POV[c], $V^{IV}O(L)$[c], V_1+PV, V_2, V_4
DMEM (t = 1 h)[d]	V_{10}, V_1+PV, V_2, V_4, V_5	–	MV-POV[c], $V^{IV}O(L)$[c], V_1+PV, V_2, V_4
DMEM (t = 3 h)[d]	V_1+PV, V_2, V_4, V_5	–	MV-POV[c], $V^{IV}O(L)$[c], V_1+PV, V_2, V_4
DMEM (t = 4 h)[d]	–	V_{10}, V_1+PV, V_2, V_4	–

[a]pH adjusted to 4; data available in [24].; [b]Data available in [31].; [c]Determined by X-band EPR, where MV-POV = Mixed-valence polyoxovanadates, in this case $[V_{18}O_{42}I]^{7-}$; $V^{IV}O^{2+}$ = $[VO(H_2O)_5]^{2+}$ and VO(L) = product formed from the V^{IV} species released from the breakage of the POV and potential ligands in the DMEM medium. The low nuclearity vanadium(V) species mentioned are: 'V_1' = $H_2VO_4^-$; 'V_2' = $H_2V_2O_7^{2-}$; 'PV' = $HVPO_7^{3-}$. V_1+PV = vanadium-phosphate complex in rapid equilibrium with V_1. [d]In this work.

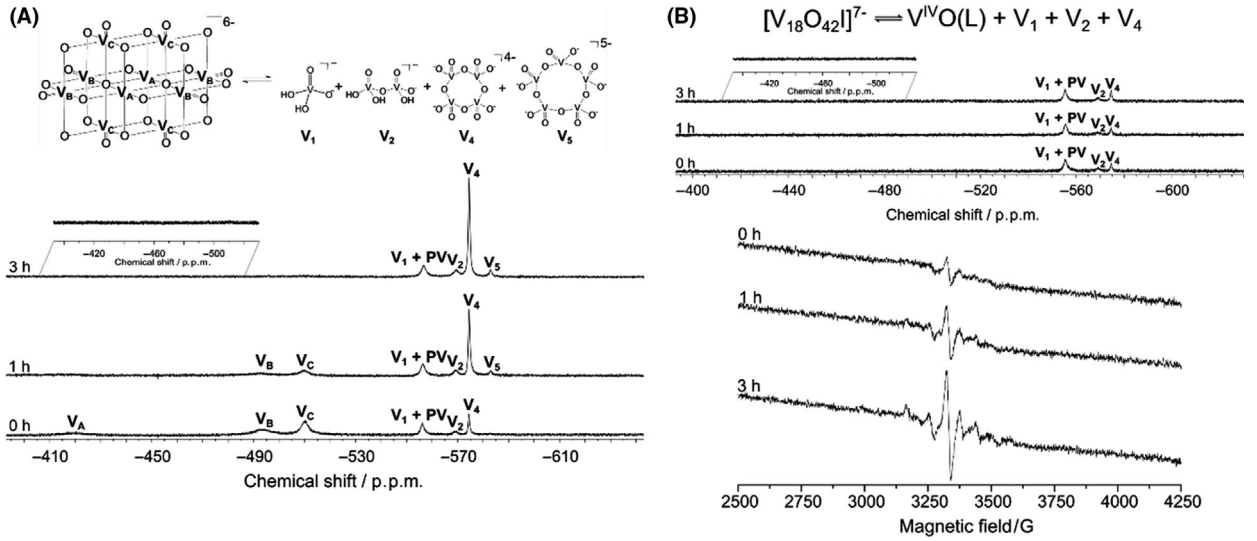

Fig. 9. ^{51}V NMR spectra recorded at 1.0 mM in DMEM at pH 7.2–7.4 for: (A) **V_{10}** and (B) **V_{18}**. The spectra at 0 h were generated from freshly prepared solutions, whereas those at 1 and 3 h were produced from each solution after incubation at 37 °C. The low nuclearity vanadium (V) species identified in the spectra were 'V_1' = $H_2VO_4^-$; 'PV' = $HVPO_7^{3-}$; 'V_2' = $H_2V_2O_7^{2-}$; 'V_4' = $V_4O_{12}^{4-}$ and 'V_5' = $V_5O_{15}^{5-}$.

ATPases [17,20]. To pursue the idea of pan-inhibition, in this work POVs were tested against the three most important ABC transporters. To the best of our knowledge, this is the first study describing the effect of POVs on human transporter proteins. Interestingly, these compounds were selective towards P-gp (Fig. 2).

After *in vitro* and *in vivo* identification of P-gp inhibitors, several clinical trials were performed using the first, second and third generations of these inhibitors [37]. Most of the studies, even using the third generation of P-gp inhibitors, failed to improve the response to chemotherapy [38]. These frustrating results could be explained in several ways. For example, various MDR mechanisms could be operating simultaneously. Also, the substrate specificities of ABC transporters clearly overlap. Another explanation is that experimental results are affected by a lack of information concerning the function and expression levels of the ABC transporters for each patient that received the P-gp inhibitors [39]. Despite the negative results from clinical trials, new evidence supports the clinical significance of ABC drug transporters. With the development of personalized medicine using current technologies, new clinical trials are necessary to investigate the clinical application of inhibitors of these transporters in combination with chemotherapy [40].

Decavanadate has been reported to modulate the human voltage-dependence of the Ca^{2+}-activated, non-

selective (CAN) ion channel TRPM4 [41]. Most recently, two decavanadate-binding sites were identified in the cytosolic domain of TRPM4, both showing a high density of positively charged residues [42]. In this work, the apparent specificity constant of P-gp was affected by $\mathbf{V_{10}}$ and $\mathbf{V_{18}}$, which suggests that there is a component of competitive inhibition. The estimated values of the competitive inhibition constants were 8.6 μM for $\mathbf{V_{10}}$ and 5.4 μM for $\mathbf{V_{18}}$ (Fig. 3B,C). It is likely that there is also a component of uncompetitive inhibition, but it is not possible to estimate this from the data, since it is not possible to obtain reliable estimates of V_{max}. In fact, it is not feasible to do the experiments at the high rhodamine concentrations that would be necessary for estimating V_{max}. This situation is not uncommon in studies of this type of transporter [43].

The *in vitro* anticancer activity of POV, including decavanadate and octadecavanadates with phosphate (V_{18}@PO_4) and water (V_{18}@H_2O) encapsulated, and their toxicity to normal cells lines have been recently revised [14]. $\mathbf{V_{18}}$ employed in this work is a new variation of the well-known mixed-valence octadecavanadate clusters that was recently reported by our group [31], and no additional studies with mammal cells have been provided yet. Regarding our findings, the cytotoxicity of NIH3T3 cells upon treatment with $\mathbf{V_{10}}$ and $\mathbf{V_{18}}$ (6.0 μM) are in the same range found for other mammalian cells, including Chinese hamster ovary (CHO) cells, IC_{50} 3.2 μM [24] and human normal hepatocytes (L02) cells, IC_{50} of 6.5 μM for $(H_2tmen)_3[V_{10}O_{28}]$ and 7.2 μM for $(H_2en)_3[V_{10}O_{28}]$, where tmen = *N*,*N*,*N*',*N*'-tetramethylethylenediamine and en = ethylenediamine [44]. On the other hand, it is widely known that the enhancement of efficacy of V_{10} can be modulated by the suitable choice of a cation, decreasing the deleterious effects on normal cells while remaining highly toxic to cancer cells [45,46].

Nowadays, it is a widely recognized fact that POMs are able to penetrate cell membranes [13,47,48]. However, the mechanism by which these large polyoxoanions do so remains obscure. The most accepted theory involves recognition of the POMs by a scavenger receptor on the cell's outer surface and subsequent cluster endocytosis [13]. It is also known that POVs, in spite of their high negative charge, have a high affinity for lipophilic surfaces, and are able to interact with a membrane's lipid bilayer [22,24]. Additionally, some evidence, such as the cytosolic-binding site of the TRPM4 channel [42] and the effect of decavanadate on mitochondrial chain enzymes support the hypothesis that POVs cross the cell membrane for different reasons [13]. However, the time-course speciation studies of $\mathbf{V_{10}}$ showed the formation of small oligomers with V_4 as the major component, making it difficult to unequivocally assign the active species. Still, this remains a controversial issue, and further studies are needed in order to clarify this matter.

Substrates of ABC drug transporters that bind to the TMDs typically trigger conformational changes in the NBDs, stimulating the ATPase activity. In addition, inhibitors also target the TMDs, but generally have an inhibitory effect on the ATPase activity, such as Zosuquidar, which binds to the TMDs and increases the distance between the NBDs, offering a plausible explanation for the inhibition of the ATPase activity in the presence of inhibitors [49]. To investigate the interaction of POVs with NBDs, an ATPase assay was carried out. It is well established that orthovanadate inhibits the ATPase activity by trapping an adenosine diphosphate (ADP) at the catalytic site, occupying the position of the γ-phosphate after ATP hydrolysis and forming a stable P-gp•ADP•V_i complex [11,36]. POVs inhibited the ATPase activity of P-gp with high affinity, showing IC_{50} values of approximately 1 μM (Table 2). The K_i values obtained by measuring the ATPase activity either in the P-gp baculovirus-infected High-Five cell membranes or using purified P-gp from KB-V1 cells and reconstituted in an artificial membrane were approximately 1–3 μM [50,51]. POVs also inhibited the ATPase activity of ABCG2 (Fig. 4A). The 10-fold lower affinity to inhibit the ATPase activity of ABCG2 *versus* P-gp (Table 2) may explain the lack of effect of POVs on the ABCG2 transport activity (Fig. 2).

Enzyme inhibition and protein-binding assays with vanadates, mostly with $\mathbf{V_1}$ and $\mathbf{V_{10}}$, are generally performed using isolated proteins, mainly ATPases [52]. The use of large POVs and MV-POVs is slowly emerging, but only a few examples are currently available, such as the interaction of phosphotetradecavanadate (PV_{14}) with Na^+/K^+ and Ca^{2+}-ATPases [53], and of $MnV_{11}O_{33}^{5-}$ and $MnV_{13}O_{38}^{7-}$ with Ca^{2+}-ATPase [54]. The inhibition of ATPase activity has also been explored with a variety of polyoxotungstates (POT) [55], as summarized in Table S3. Despite these findings, the variations in proteins and in protocols render comparisons somewhat ambiguous and any conclusion should be drawn with caution. The IC_{50} values for the P-gp ATPase activity for $\mathbf{V_{10}}$ and $\mathbf{V_{18}}$ (1.26 μM) are close to the lowest values found for PV_{14} for Na^+/K^+-ATPase (1.4 μM), and also for POT $[H_{10}Se_2W_{29}O_{103}]^{14-}$ and $[\alpha\text{-}P_2W_{18}O_{62}]^{6-}$ (0.3 and 0.6 μM) in the inhibition of Ca^{2+}-ATPase. It is important to note that the IC_{50} values of the ATPase activity by POVs in studies with isolated proteins were below 60 μM [17,52,53], while a broader range of IC_{50}

values (from 0.3 to 200 μM) was found for POT [55], suggesting a higher dependence on the composition, shape and charge of the latter class of POM.

To elucidate the molecular mechanism of inhibition, the effect of POVs was evaluated on the binding of a conformational antibody (17F9) that recognizes an extracellular region of P-gp. Interestingly, the two best-performing compounds, **V_{10}** and **V_{18}**, showed different patterns (Fig. 4C), suggesting that these complexes can trigger different conformational changes at the protein level, either by binding at different sites or by producing other vanadium species that, in principle, could also be active. Before investigating the speciation of POVs in the culture medium, a time-course inhibition experiment was performed. The results suggested that the POVs do not easily cross the cell membrane (Fig. 5A), since the P-gp inhibition was time-dependent. To confirm this finding, a POV containing a fluorescent dye (Rhodamine B) not transported by P-gp was synthesized and characterized in this study. The intracellular accumulation of this compound (**RhoB-V_{10}**) confirmed the effect to be time-dependent (Fig. 8A).

Speciation studies of POV in DMEM

The stability studies of POMs in solution and under physiological conditions, as well as the establishment of the chemical equilibria in the time course of biological assays is crucial to allow for proper structure-activity correlations [56]. The speciation of POVs was investigated in culture medium for a period of time corresponding to the achievement of maximum inhibition of P-gp activity. In the case of **V_{10}**, the formation of $[HV_{10}O_{28}]^{5-}$, V_1+PV, V_2 and V_4 was observed by ^{51}V NMR spectroscopy (Fig. 9A), demonstrating the fragmentation of the polyoxoanion. After 3 h of incubation, the three signals corresponding to the monoprotonated $[HV_{10}O_{28}]^{5-}$ species disappeared, and an increase in V_4, along with the appearance of V_5, was observed (Fig. 8B). In a previous study with CHO cell cultures, it was demonstrated that in DMEM medium V_4 remains the predominant species even after 24 h of incubation [24]. In sharp contrast, **V_{18}** was mostly stable in DMEM. These differences could explain the different effects of **V_{10}** and **V_{18}** on conformational antibody binding (Fig. 4C). The two distinct cell populations observed on cell exposition to **V_{10}** could be partially associated with the species formed by this POV in the culture medium, supporting our hypothesis that **V_{10}** and **V_{18}** have different P-gp binding sites, probably located on the NBDs due to the high negative charge of these compounds.

According to the literature, POVs appear to be the next-generation metallodrugs used for cancer treatment [13,14], and the ability to circumvent the multidrug resistance mediated by P-gp increases their potential as anticancer agents. In addition, P-gp inhibition can open new avenues to study pharmacological combinations of POVs with different cancer drugs. Finally, ABC transporter inhibitors are commonly highly hydrophobic compounds that target the drug binding site at TMDs, a protein region rich in hydrophobic amino acid residues. The hydrophobicity of ABC transporter inhibitors imposes solubility barriers for pre-clinical tests on drug development. In this context, the water solubility of **V_{10}** and **V_{18}** represents a desirable feature. Also, the hydrophilic nature of the POVs supports the hypothesis that these compounds target an unusual binding site on P-gp, and this possibility deserves further attention.

Conclusion

This is the first study describing the interaction of POVs with the human ABC transporters known to be associated with the development of MDR. POVs are selective inhibitors of the transport function of P-gp and their intracellular accumulation is time-dependent. Compounds **V_{10}** and **V_{18}** are the most promising. However, effort must still be made to overcome their cytotoxicity and to better understand their mechanisms of action, along with the species involved. The safe use of a POM, and more specifically a POV, with optimization of therapeutic effects and minimization of side effects requires an exhaustive evaluation of its reactivity, determination of mechanisms of action and correlation with specific biological conditions.

Methods

Materials

Rhodamine 123, mitoxantrone, GF120918 (Elacridar), Ko143, Verapamil and MTT were purchased from Sigma-Aldrich (San Luis, MO, USA). All other reagents were commercial products of the highest available purity.

Cell cultures

Mouse fibroblast NIH3T3 parental cells (wild-type) and NIH3T3 cells stably transfected with ABCB1 (NIH3T3/P-gp), human fibroblast HEK293 parental cells (wild-type) and HEK293 cells stably transfected with ABCG2 (HEK293/ABCG2), hamster fibroblast BHK-21 parental cells (wild-type) and BHK-21 cells stably transfected with

ABCC1 (BHK-21/MRP1) were all kindly provided by Dr. Attilio Di Pietro (IBCP, Lyon, France). All cells were maintained in Dulbecco's Modified Eagle's Medium (DMEM high glucose) supplemented with 10% foetal bovine serum (FBS), 1% penicillin/streptomycin, and with either 0.75 mg·mL^{-1} G418 (HEK293/ABCG2), 60.0 ng·mL^{-1} colchicine (NIH3T3/P-gp) or 0.10 mg·mL^{-1} methotrexate (BHK-21/ABCC1) at 37 °C in 5% CO_2 atmosphere.

Inhibition assay

The ability of compounds to inhibit the transport function of ABC proteins was evaluated using fluorescent substrates by flow cytometry. Cells were seeded at a density of 1.0×10^5 cells per well in 24-well culture plates and allowed to attach for 48 h at 37 °C in 5% CO_2 atmosphere. Parental and transfected cells were exposed to fluorescent substrates with or without compounds at different concentrations, and incubated at 37 °C in 5% CO_2 for 30 min. The cells were then washed with 300.0 µL of PBS. One drop of trypsin-EDTA was added and the mixture was incubated until cells detached. The cells were suspended in 300.0 µL of ice-cold PBS and kept on ice until flow cytometry analysis. Intracellular substrate fluorescence data were acquired using a FACSCalibur flow cytometer equipped with two lasers (488 and 635 nm). At least 10 000 events were collected, and Rhodamine 123 and mitoxantrone median fluorescence intensities were recorded in FL1-H and FL4-H channels, respectively. The inhibition percentage was calculated using parental cells or a reference inhibitor.

Antibody binding

The effect on the binding of a conformational antibody was determined by flow cytometry. NIH3T3-P-gp cells were cultivated at 37 °C in 5% CO_2 until approximately 90% of confluence, then detached and separated in tubes with 2.5×10^5 cells per sample. Cells were centrifuged at 1000 ***g*** for 3 min and the supernatant was discarded. The resulting cell pellet was suspended in PBS (100.0 µL), and 4.0 µL of BSA solution (stock 1.0 mg·mL^{-1}) was added to each sample. Samples were incubated with: Rhodamine 123 (5.0 µM), GF120918 (1.0 µM), $\mathbf{V_{10}}$ (50.0 µM) and $\mathbf{V_{18}}$ (50.0 µM) for 10 min at 37 °C. After this period of time, the primary antibody anti-human P-glycoprotein clone 17F9 (BD Pharmingen Cat. 557001 – dilution 1 : 100) was added to each sample, and the mixture was incubated for 30 min at 37 °C. Cells were centrifuged (1000 ***g***, 3 min) and the supernatant was discarded. Cells were suspended in PBS (100.0 µL) and the secondary antibody was added [anti-mouse PE, Abcam (Cambridge, UK) Cat. Ab97024 – dilution 1 : 200]. The samples were incubated at 37 °C for 30 min, centrifuged, and the cell pellet was suspended in 300.0 µL of PBS. Data were recorded by flow cytometry FACSCalibur using the FL-2 channel. At least 10 000 events were collected.

ATPase activity

The ATPase activity assay was performed as previously described [57]. High-Five insect cell total membranes overexpressing ABCB1 (P-gp) were used at a concentration of 10.0 µg protein/tube, and ABCG2 at a concentration of 5.0 µg protein/tube, in a final volume of 100.0 µL. The High-Five membranes were incubated in assay buffer containing 50.0 mM of Tris-HCl, pH 6.8, 150.0 mM of *N*-methyl-D-glucamine (NMDG)-Cl, 5.0 mM of sodium azide, 1.0 mM of EGTA, 1.0 mM of ouabain, 2.0 mM of DTT, and 10.0 mM of $MgCl_2$, in the presence or absence of sodium orthovanadate (0.30 mM). The master mix (protein + assay buffer) was incubated with the POVs at increasing concentrations (0.05–2.5 mM) for 20 min at 37 °C in the presence of ATP (5.0 mM). The reaction was stopped with the addition of 100.0 µL of 5% SDS, 400.0 µL of P_i solution (sulphuric acid, water, ammonium molybdate and antimony potassium tartrate) for colour development and 200.0 µL of 1% ascorbic acid. The absorbance was measured after 10 min at 880 nm using a spectrophotometer Ultrospec 3100 pro (Amersham Biosciences, Amersham, UK).

Chemicals and solutions

All syntheses employed ultrapure water (MilliQ, Darmstadt, Germany, Millipore type 1, 18.2 MΩ cm resistivity at 25 °C). $NaVO_3$ (98.0%) was purchased from Aldrich and Rhodamine B (RhoB, $C_{28}H_{31}ClN_2O_3$ – analytical standard) from Merck (Darmstadt, Germany). Sodium decavanadate $[\{Na_6(H_2O)_{20}V_{10}O_{28}\cdot 4H_2O\}_n]$ ($\mathbf{V_{10}}$) [58], $K(NH_4)_4[H_6V_{14}O_{38}(PO_4)]\cdot 11H_2O$ ($\mathbf{V_{14}}$) [59], $(Me_4N)_6[V_{15}O_{36}Cl]$ ($\mathbf{V_{15}}$) [60], and $(NH_4)_2(Me_4N)_5[V_{18}O_{42}I]\cdot Me_4NI\cdot 5H_2O$ ($\mathbf{V_{18}}$) [31] were prepared as previously described. For the biological assays, 10.0 mM aqueous stock-solutions of $\mathbf{V_{10}}$ (pH adjusted to 4 with diluted HCl), $\mathbf{V_{14}}$ (pH = 4.2), $\mathbf{V_{15}}$ (pH = 6.3) and $\mathbf{V_{18}}$, pH = 6.0) were prepared immediately before use. A 10.0-mM stock-solution of $\mathbf{RhoB\text{-}V_{10}}$ was prepared in dmso.

Analytical methods

Carbon, hydrogen and nitrogen percentages were determined on a Perkin Elmer – CHN 2400 Elemental Analyzer, while the vanadium content was obtained by gravimetric analysis. An FTIR MB-BOMEN spectrophotometer was used to register the infrared spectra (4000–400 cm^{-1}) from KBr pellets. A Netzsch STA449 F3 Jupiter analyzer equipped with a silicon carbide furnace and dinitrogen as carrier gas was the instrument used for collecting thermogravimetric (TGA) data. A sample (*ca.* 4 mg) was heated in an aluminium pan in the range of 25–800 °C at

10 °C min^{-1}. X-band (9.5 GHz) EPR spectra were recorded at 77 K from solutions in water and DMEM using a Bruker ELEXSYS E-500 spectrometer. ^{51}V NMR spectra were obtained from a Bruker 400 MHz Avance III spectrometer (9.4 T) equipped with a multinuclear direct detection probe (5 mm), using calibrated 90° pulses, 2048 scans, a recycling delay of 0.100 s, acquisition times of 0.218 s and a spectral width of 714 ppm. The ^{51}V nucleus was detected at 105.2 MHz, and $VOCl_3$ (neat, capillary) was used as a reference (0.00 ppm). Spectral intensities were normalized on each experiment by comparison with the reference signal.

Preparation of $(RhoBH)_4[H_2V_{10}O_{28}]\cdot 2RhoB\cdot 14H_2O$ (RhoB-V_{10})

A suspension of $NaVO_3$ (0.610 g, 5.00 mmol) in 30 mL of water was heated at 90 °C for five minutes under magnetic stirring. After cooling down to room temperature, the pH of the resulting colourless solution was adjusted to 4.0 with diluted HCl, yielding an orange solution. Then, a sonicated solution of Rhodamine B (0.240 g, 0.50 mmol) in 30 mL of water was slowly added, forming an overlayer. After seven days, the dark-green crystals formed were filtered off, washed twice with 2.0 mL of cold water, and dried under vacuum (**RhoB-V_{10}**, 1.17 g, 61% yield based on $NaVO_3$). Product **RhoB-V_{10}** was soluble in dmso and partially soluble in water and ethanol. Elemental analysis values calculated for $C_{168}H_{214}N_{12}O_{60}V_{10}$: C 52.13; H 5.57; N 4.34; V 13.16%. Found: C 51.40; H 5.21; N 4.37; V 13.04%. FTIR (KBr, cm^{-1}, s = strong, m = medium, w = weak): 1649(w), 1589(s), 1468(m), 1413(m), 1336(m), 1275(m), 1248(m), 1180(m), 1132(m), 1074(m), 972(m), 825(w), 756(w).

Single crystal X-ray diffraction analysis

From a sample under oil, one dark-green prism of *ca* 0.218 × 0.113 × 0.046 mm^3 was mounted on a Micromount/mesh and fixed in cold nitrogen stream on a Bruker D8 Venture diffractometer equipped with a Photon 100 CMOS detector, Mo-Kα radiation and graphite monochromator. Intensity data were measured by thin-slice ω- and φ-scans. Data were processed using the APEX3 program [61]. The structure was determined by the intrinsic phasing method routines in the SHELXT program [28] and refined by the full-matrix least-squares method, on F^2's, in SHELXL [62]. Complete data collection and refinement information can be found in Table S1 and the main hydrogen bonds that permeate the crystal packing of the structure are listed in Table S2. The non-hydrogen atoms were refined with anisotropic thermal parameters. All hydrogen atoms were modelled in idealized positions with U(iso)'s set at 1.2*U(eq) or, for the methyl group hydrogen atoms, 1.5*U(eq) of the parent carbon atoms, except for those belonging to cations (H59 and H92), to one crystallization water molecule (H1W5 and H2W5), and to the decavanadate anion (H11). These H atoms were located in difference maps and distance restraints (DFIX and DANG) were applied to them. Computer programs used in this analysis were noted above and were run through WinGX [63].

^{51}V NMR and EPR spectroscopies in DMEM

V_{10}, **RhoB-V_{10}** and **V_{18}** solutions in culture medium were analysed by ^{51}V NMR spectroscopy. Aqueous stock-solutions of **V_{10}** and **V_{18}** were prepared at 10.0 mM, and the pH of **V_{10}** was adjusted to 4.0 with diluted HCl. A 10.0-mM stock-solution of **RhoB-V_{10}** was prepared in dmso. Sample preparation was carried out using a 50.0 μL aliquot of each stock-solution diluted in 400.0 μL of DMEM, with the addition of 50.0 μL of D_2O, resulting in a final concentration of 1.0 mM for each polyoxovanadate. Spectra were acquired at room temperature from freshly prepared samples and after 3 h of incubation at 37 °C, while **RhoB-V_{10}** spectra were generated from freshly prepared samples and after 4 h of incubation at 37 °C. EPR spectra were also recorded from a frozen **V_{18}** sample in DMEM at 1.0 mM before (0 h) and after 1 and 3 h of incubation at 37 °C.

Acknowledgements

The authors thank Jaśa Fernandes Soares for design some chemical experiments and the critical reading of the manuscript. They thank Attilio Di Pietro, IBCP Lyon – France, for providing the stably transfected cell lines, and George Leiman for editing this manuscript. This project was supported by the Brazilian Research Council (CNPq, grant number 400953/2016-1) and Fundação Araucária (Code 006 – 09/2016). This study was also financed in part by the Coordenação de Aperfeiçoamento de Pessoal de Nível Superior - Brasil (CAPES) – Finance Code 001 and CAPES PrInt UFPR. DHK and SVA were supported by the Intramural Research Program, National Institutes of Health, National Cancer Institute, Center for Cancer Research.

Author contributions

GV, VRM and SVA designed the biological experiments. GGN designed the chemical experiments. DHK, GAA, IFZ and ISZ performed the biological experiments. FGMR and EMS helped with the data analysis. DAM and VRM performed the kinetic analysis. GP performed the statistical analysis. JMM, KP, VKB and FSS performed the synthesis and characterization of the compounds. GV and GGN wrote the manuscript. Both students (Diogo Henrique Kita and Gisele Alves de Andrade) contributed equally to this work.

Supplementary data

Supplementary data associated with this article can be found in the online version. CCDC: 2120954 can be obtained at http://www.ccdc.cam.ac.uk/structures.

Data accessibility

The data that supports the findings of this study are available in Figs 2–9/Tables 1–4 and the supplementary material of this article.

References

1 Dassa E, Bouige P. The ABC of ABCs: a phylogenetic and functional classification of ABC systems in living organisms. *Res Microbiol*. 2001;**152**:211–29.
2 Saurin W, Hofnung M, Dassa E. Getting in or out: early segregation between importers and exporters in the evolution of ATP-binding cassette (ABC) transporters. *J Mol Evol*. 1999;**48**:22–41.
3 Dean M, Rzhetsky A, Allikmets R. The human ATP-binding cassette (ABC) transporter superfamily. *Genome Res*. 2001;**11**:1156-66.
4 Linton KJ, Linton KJ. Structure and function of ABC transporters. *Physiology (Bethesda)*. 2007;**22**:122–30.
5 Szakács G, Paterson JK, Ludwig JA, Booth-genthe C. Targeting multidrug resistance in cancer. *Nat Rev Drug Discov*. 2006;**5**:219–34.
6 Juliano RL, Ling V. A surface glycoprotein modulating drug permeability in Chinese hamster ovary cell mutants. *BBA Biomembr*. 1976;**455**:152–62.
7 Cole SPC, Bhardwaj G, Gerlach JH, Mackie JE, Grant CE, Almquist KC et al. Overexpression of a transporter gene in a multidrug-resistant human lung cancer cell line. *Science*. 1992;**258**:1650–4.
8 Allikmets R, Schriml LM, Hutchinson A, Romano-Spica V, Dean M. A human placenta-specific ATP-binding cassette gene (ABCP) on chromosome 4q22 that is involved in multidrug resistance. *Cancer Res*. 1998;**58**:5337–9.
9 Doyle LA, Yang WD, Abruzzo LV, Krogmann T, Gao YM, Rishi AK et al. A multidrug resistance transporter from human MCF-7 breast cancer cells. *Proc Natl Acad Sci USA*. 1998;**95**:15665–70.
10 Miyake K, Mickley L, Litman T, Zhan ZR, Robey R, Cristensen B et al. Molecular cloning of cDNAs which are highly overexpressed in mitoxantrone-resistant cells: demonstration of homology to ABC transport genes. *Cancer Res*. 1999;**59**:8–13.
11 Bársony O, Szalóki G, Türk D, Tarapcsák S, Gutay-Tóth Z, Bacsó Z et al. A single active catalytic site is sufficient to promote transport in P-glycoprotein. *Sci Rep*. 2016;**6**:24810.
12 Tamaki A, Ierano C, Szakacs G, Robey RW, Bates SE. The controversial role of ABC transporters in clinical oncology. *Essays Biochem*. 2011;**50**:209–32.
13 Bijelic A, Aureliano M, Rompel A. Polyoxometalates as potential next-generation metallodrugs in the combat against cancer. *Angew Chem Int Ed Engl*. 2019;**58**:2980–99.
14 Aureliano M, Gumerova NI, Sciortino G, Garribba E, Rompel A, Crans DC. Polyoxovanadates with emerging biomedical activities. *Coord Chem Rev*. 2021;**447**:214143.
15 Gu Y, Li Q, Huang Y, Zhu Y, Wei Y, Ruhlmann L. Polyoxovanadate-iodobodipy supramolecular assemblies: new agents for high efficiency cancer photochemotherapy. *Chem Commun*. 2020;**56**:2869–72.
16 Soares SS, Martins H, Duarte RO, Moura JJG, Coucelo J, Gutiérrez-Merino C et al. Vanadium distribution, lipid peroxidation and oxidative stress markers upon decavanadate in vivo administration. *J Inorg Biochem*. 2007;**101**:80–8.
17 Pezza RJ, Villarreal MA, Montich GG, Argaraña CE. Vanadate inhibits the ATPase activity and DNA binding capability of bacterial MutS. A structural model for the vanadate-MutS interaction at the Walker A motif. *Nucleic Acids Res*. 2002;**30**:4700–8.
18 Zebisch M, Krauss M, Schäfer P, Sträter N. Structures of *Legionella pneumophila* NTPDase1 in complex with polyoxometallates. *Acta Crystallogr Sect D Biol Crystallogr*. 2014;**70**:1147–54.
19 Marques MPM, Gianolio D, Ramos S, Batista De Carvalho LAE, Aureliano M. An EXAFS approach to the study of polyoxometalate-protein interactions: the case of decavanadate-actin. *Inorg Chem*. 2017;**56**:10893–903.
20 Aureliano M, Fraqueza G, Ohlin CA. Ion pumps as biological targets for decavanadate. *Dalt Trans*. 2013;**42**:11770–7.
21 Ramos S, Manuel M, Tiago T, Duarte R, Martins J, Gutiérrez-Merino C et al. Decavanadate interactions with actin: Inhibition of G-actin polymerization and stabilization of decameric vanadate. *J Inorg Biochem*. 2006;**100**:1734–43.
22 Al-Qatati A, Fontes FL, Barisas BG, Zhang D, Roess DA, Crans DC. Raft localization of Type I Fcε receptor and degranulation of RBL-2H3 cells exposed to decavanadate, a structural model for V2O5. *J Chem Soc Dalt Trans*. 2013;**42**:11912–20.
23 Crans DC, Peters BJ, Wu X, McLauchlan CC. Does anion-cation organization in Na+-containing X-ray crystal structures relate to solution interactions in inhomogeneous nanoscale environments: sodium-decavanadate in solid state materials, minerals, and microemulsions. *Coord Chem Rev*. 2017;**344**:115–30.
24 Althumairya D, Postal K, Barisas G, Gioppo Nunes G, Roess DA, Crans DC. Polyoxometalates function as indirect activators of a G protein-coupled receptor. *Metallomics*. 2020;**12**:1044–61.

25 Kioseoglou E, Petanidis S, Gabriel C, Salifoglou A. The chemistry and biology of vanadium compounds in cancer therapeutics. *Coord Chem Rev*. 2015;**301–302**:87–105.
26 Rees DC, Johnson E, Lewinson O. ABC transporters: the power to change. *Nat Rev Mol Cell Biol*. 2010;**10**:80799.
27 Eytan GD, Regev R, Oren G, Hurwitz CD, Assaraf YG. Efficiency of P-glycoprotein-mediated exclusion of rhodamine dyes from multidrug-resistant cells is determined by their passive transmembrane movement rate. *Eur J Biochem*. 1997;**248**:104–12.
28 Boşnjaković-Pavlović N, Prévost J, Spasojević-De Biré A. Crystallographic statistical study of decavanadate anion based-structures: toward a prediction of noncovalent interactions. *Cryst Growth Des*. 2011;**11**:3778–89.
29 Wang P, Cheng M, Zhang Z. On different photodecomposition behaviors of rhodamine B on laponite and montmorillonite clay under visible light irradiation. *J Saudi Chem Soc*. 2014;**18**:308–16.
30 Postal K, Maluf DF, Valdameri G, Rüdiger AL, Hughes DL, De Sá EL et al. Chemoprotective activity of mixed valence polyoxovanadates against diethylsulphate in *E. coli* cultures: insights from solution speciation studies. *RSC Adv*. 2016;**6**:114955–68.
31 Postal K, Santana FS, Hughes DL, Rüdiger AL, Ribeiro RR, Sá EL et al. Stability in solution and chemoprotection by octadecavanadates(IV/V) in *E. coli* cultures. *J Inorg Biochem*. 2021;**219**:111438.
32 Rehder D, Polenova T, Bühl M. Vanadium-51 NMR. *Annu Rep NMR Spectrosc*. 2007;**62**:49–114.
33 Samart N, Arhouma Z, Kumar S, Murakami HA, Crick DC, Crans DC. Decavanadate inhibits mycobacterial growth more potently than other oxovanadates. *Front Chem*. 2018;**6**:1–16.
34 Iannuzzi MM, Rieger PH. Nature of vanadium(IV) in basic aqueous solution. *Inorg Chem*. 1975;**14**:2895–9.
35 Higgins CF. ABC transporters: physiology, structure and mechanism – an overview. *Res Microbiol*. 2001;**152**:205–10.
36 Senior AE, Al-Shawi MK, Urbatsch IL. The catalytic cycle of P-glycoprotein. *FEBS Lett*. 1995;**377**:285–9.
37 Leonard GD, Fojo T, Bates SE. The role of ABC transporters in clinical practice. *Oncologist*. 2003;**8**:411–24.
38 Binkhathlan Z, Lavasanifar A. P-glycoprotein inhibition as a therapeutic approach for overcoming multidrug resistance in cancer: current status and future perspectives. *Curr Cancer Drug Targets*. 2013;**13**:326–46.
39 Robey RW, Massey PR, Amiri-Kordestani L, Bates SE. ABC transporters: unvalidated therapeutic targets in cancer and the CNS. *Anticancer Agents Med Chem*. 2011;**10**:625–33.
40 Robey RW, Pluchino KM, Hall MD, Fojo AT, Bates SE, Gottesman MM. Revisiting the role of ABC transporters in multidrug-resistant cancer. *Nat Rev Cancer*. 2018;**18**:452–64.
41 Nilius B, Prenen J, Janssens A, Voets T, Droogmans G. Decavanadate modulates gating of TRPM4 cation channels. *J Physiol*. 2004;**560**:753–65.
42 Winkler PA, Huang Y, Sun W, Du J, Lü W. Electron cryo-microscopy structure of a human TRPM4 channel. *Nature*. 2017;**552**:200–5.
43 Saengkhae C, Loetchutinat C, Garnier-Suillerot A. Kinetic analysis of rhodamines efflux mediated by the multidrug resistance protein (MRP1). *Biophys J*. 2003;**85**:2006–14.
44 Li YT, Zhu CY, Wu ZY, Jiang M, Yan CW. Synthesis, crystal structures and anticancer activities of two decavanadate compounds. *Transit Met Chem*. 2010;**35**:597–603.
45 Galani A, Tsitsias V, Stellas D, Psycharis V, Raptopoulou CP, Karaliota A. Two novel compounds of vanadium and molybdenum with carnitine exhibiting potential pharmacological use. *J Inorg Biochem*. 2015;**142**:109–17.
46 Shah HS, Al-Oweini R, Haider A, Kortz U, Iqbal J. Cytotoxicity and enzyme inhibition studies of polyoxometalates and their chitosan nanoassemblies. *Toxicol Rep*. 2014;**1**:341–52.
47 Yamase T. Anti-tumor, -viral, and -bacterial activities of polyoxometalates for realizing an inorganic drug. *J Mater Chem*. 2005;**15**:4773.
48 Sakamoto A, Unoura K, Nabika H. Molecular scale insights into activity of polyoxometalate as membrane-targeting nanomedicine from single-molecule observations. *J Phys Chem C*. 2018;**122**:1404–11.
49 Alam A, Kowal J, Broude E, Roninson I, Locher KP. Structural insight into substrate and inhibitor discrimination by human P-glycoprotein. *Science*. 2019;**363**:753–6.
50 Sarkadi B, Price EM, Boucher RC, Germann UA, Scarborough GA. Expression of the human multidrug resistance cDNA in insect cells generates a high activity drug-stimulated membrane ATPase. *J Biol Chem*. 1992;**267**:4854–8.
51 Ambudkar SV, Lelong IH, Zhang J, Cardarelli CO, Gottesman MM, Pastan I. Partial purification and reconstitution of the human multidrug-resistance pump: characterization of the drug-stimulatable ATP hydrolysis. *Proc Natl Acad Sci USA*. 1992;**89**:8472–6.
52 Fraqueza G, Batista De Carvalho LAE, Marques MPM, Maia L, Ohlin CA, Casey WH et al. Decavanadate, decaniobate, tungstate and molybdate interactions with sarcoplasmic reticulum Ca2+-ATPase: Quercetin prevents cysteine oxidation by vanadate but does not reverse ATPase inhibition. *Dalt Trans*. 2012;**41**:12749–58.
53 Fraqueza G, Fuentes J, Krivosudský L, Dutta S, Mal SS, Roller A et al. Inhibition of Na + /K + - and Ca 2+ -ATPase activities by phosphotetradecavanadate. *J Inorg Biochem*. 2019;**197**:110700.

54 Marques-Da-Silva D, Fraqueza G, Lagoa R, Vannathan AA, Mal SS, Aureliano M. Polyoxovanadate inhibition of: *Escherichia coli* growth shows a reverse correlation with Ca2+-ATPase inhibition. *New J Chem*. 2019;**43**:17577–87.
55 Gumerova N, Krivosudský L, Fraqueza G, Breibeck J, Al-Sayed E, Tanuhadi E et al. The P-type ATPase inhibiting potential of polyoxotungstates. *Metallomics*. 2018;**10**:287–95.
56 Gumerova NI, Rompel A. Polyoxometalates in solution: Speciation under spotlight. *Chem Soc Rev*. 2020;**49**:7568–601.
57 Ambudkar SV. Drug-stimulatable ATPase activity in crude membranes of human MDR1- transfected mammalian cells. *Methods Enzymol*. 1998;**292**:504–14.
58 Yerra S, Tripuramallu BK, Das SK. Decavanadate-based discrete compound and coordination polymer: synthesis, crystal structures, spectroscopy and nano-materials. *Polyhedron*. 2014;**81**:147–53.
59 Postal K, Maluf DF, Valdameri G, Hughes DL, Ribeiro RR, De SEM et al. RSC advances chemoprotective activity of mixed valence polyoxovanadates against diethylsulphate in *E. coli*. *RSC Adv*. 2016;**6**:114955–68.
60 Nunes GG, Bonatto AC, De Albuquerque CG, Barison A, Ribeiro RR, Back DF et al. Synthesis, characterization and chemoprotective activity of polyoxovanadates against DNA alkylation. *J Inorg Biochem*. 2012;**108**:36–46.
61 Program APEX3 (2015)
62 Sheldrick GM. Crystal structure refinement with SHELXL. *Acta Crystallogr Sect C Struct Chem*. 2015;**71**:3–8.
63 Farrugia LJ. ORTEP III for Windows. *J Appl Cryst*. 2012;**45**:849-54.

Supporting information

Additional supporting information may be found online in the Supporting Information section at the end of the article.

Fig. S1. IC_{50} inhibition curves of $\mathbf{V_{14}}$ and $\mathbf{V_{15}}$.
Fig. S2. (**A**) ORTEP diagram of the doubly-protonated decavanadate anion and the crystallographically independent Rhodamine B zwitterion in the structure of $(RhoBH)_4[H_2V_{10}O_{28}]\cdot 2RhoB\cdot 14H_2O$ (**RhoB-$\mathbf{V_{10}}$**), with the atom numbering scheme. Hydrogen atoms have been omitted for clarity, except for those belonging to the decavanadate anion. Thermal ellipsoids are drawn at the 50% probability level. (**B**) Hydrogen bonds involving the water molecule containing atom O (5W), both crystallographically independent Rhodamine B cations and the crystallographically independent Rhodamine B zwitterion. Thermal ellipsoids are drawn at the 50% probability level. These hydrogen bonds are further described in Table S2.
Fig. S3. Solution equilibrium between the cationic (left) and zwitterionic (right) forms of Rhodamine B.
Fig. S4. Thermogravimetric analysis (TGA) profile obtained for $(RhoBH)_4[H_2V_{10}O_{28}]\cdot 2RhoB\cdot 14H_2O$ (**RhoB-$\mathbf{V_{10}}$**), with $N_2\backslash O_2$ as carrier gas and temperature range of 25 to 800°C.
Fig. S5. Infrared absorption spectrum recorded for **RhoB-$\mathbf{V_{10}}$** in KBr pellets.
Fig. S6. ^{51}V NMR spectra recorded at room temperature for **RhoB-$\mathbf{V_{10}}$**, $(RhoBH)_4[H_2V_{10}O_{28}]\cdot 2RhoB\cdot 14H_2O$, in a dmso-$d_6$ solution at 1.0 mM.
Fig. S7. ^{51}V NMR spectrum recorded at room temperature for a fresh solution of $\mathbf{V_{18}}$, $(NH_4)_2(Me_4N)_5[V_{18}O_{42}I]\cdot Me_4NI\cdot 5H_2O$, in D_2O solution at 1.0 mM.
Fig. S8. Representation of the system for the purpose of modeling.
Table S1. Crystal data and structure refinement for $(RhoBH)_4[H_2V_{10}O_{28}]\cdot 2RhoB\cdot 14H_2O$.
Table S2. Relevant hydrogen bonds in the crystal structure of $(RhoBH)_4[H_2V_{10}O_{28}]\cdot 2RhoB\cdot 14H_2O$, with distances in Å and angles in degrees*.
Table S3. Inhibition of the activity of certain isolated proteins by polyoxometalates.
Data S1. Model for estimation of the effective inhibition constants of the polyoxovanadate inhibitors.